An improved selective excitation double Mössbauer spectrometer

J. van Lierop[a] and D. H. Ryan
Physics Department and Centre for the Physics of Materials, McGill University, 3600 University Street, Montreal, Quebec H3A 2T8, Canada

(Received 18 October 2000; accepted for publication 23 May 2001)

The design, operation and performance of a selective excitation double Mössbauer (SEDM) spectrometer are described. An innovative drive-mounted conversion electron detector for scattered γ-ray energy analysis provides a three orders of magnitude improvement in counting efficiency over previous SEDM equipment. Simple digital circuitry together with Wissel Mössbauer velocity transducers and electronics supplies energy synchronization for indefinite collection times. Magnetic materials containing resonant Mössbauer nuclei (e.g., ^{57}Fe) can now be conveniently studied using SEDM, offering a unique insight into dynamic processes. © *2001 American Institute of Physics.* [DOI: 10.1063/1.1386900]

I. INTRODUCTION

Conventional ^{57}Fe transmission Mössbauer experiments have been used to study various dynamic phenomena including diffusion, paramagnetic and superparamagnetic relaxation as well as spin–spin and spin–lattice relaxation. This technique is usually simple to employ, however, resulting spectra often suffer from interpretational difficulties as different physical behavior can result in the same line shape. The archetypical example of this is provided by Fe–Ni alloys where models based on two-level spin flip relaxation and static chemical disorder describe the spectra equally well.[1,2]

This dilemma is inherent to measuring incoming *or* outgoing photons during a transmission Mössbauer or single-drive scattering experiments. These methods detect what is essentially the absorption cross section of resonant Mössbauer nuclei. These resonant nuclei can be affected by time dependent hyperfine interactions as well as static perturbations such as internal field inhomogeneities from static disorder. Unfortunately, both static disorder and slow time dependent effects result in spectral line broadening. The many lines present in regular Mössbauer spectra make separating these two influences difficult.

If the effects of both incoming *and* outgoing photons are measured, the differential cross section of resonant nuclei is determined. Resonant nuclei affected by time dependent hyperfine interactions have differential cross sections that are distinct from those which are affected by static perturbations. Unique spectral characteristics will be provided by time dependent and static hyperfine interactions.

Selective excitation double Mössbauer (SEDM) spectroscopy measures the differential cross section of resonant nuclei. Two Mössbauer resonant scattering events provide a signal from resonant nuclei in the sample. The first resonant event pumps a selected transition of the hyperfine nuclear structure and populates a specific excited state. The second resonant event occurs during the de-excitation of a nucleus back into the ground state. In a material with a single, static hyperfine field (e.g., α-Fe), SEDM spectra are produced by the following: Say the $m_g=-\frac{1}{2}\rightarrow m_e=-\frac{3}{2}$ transition (see Fig. 1) is pumped. After the lifetime of the Mössbauer nucleus, a de-excitation via the $m_e=-\frac{3}{2}\rightarrow m_g=-\frac{1}{2}$ transition occurs. A single, sharp line (see line No. 1 in Fig. 2) is the result. If the $m_g=-\frac{1}{2}\rightarrow m_e=-\frac{1}{2}$ transition is pumped, de-excitation through the $m_e=-\frac{1}{2}\rightarrow m_e=-\frac{1}{2}$ and $m_e=-\frac{1}{2}\rightarrow m_g=\frac{1}{2}$ transitions will occur. Two sharp lines whose intensities are proportional to the cross sections of the respective transitions is the outcome (Fig. 2).

Time dependent hyperfine interactions in a material allow Mössbauer nuclei to exchange energy with their surroundings. If this energy exchange occurs during the lifetime of an excited nucleus, new levels will be populated and *extra* transitions will be observed. The SEDM spectra will exhibit these new lines. A SEDM spectrum of a material exhibiting time dependent effects will contain information about the relaxation process and its rate.

At temperatures below which relaxation can occur, SEDM spectra will show the effects, if there are any, of static hyperfine perturbations with spectral linewidths which are broader than those measured from a sample with a single hyperfine field. With increasing temperature, slow dynamic effects will provide new spectral lines. In this manner it is possible to clearly differentiate between static and dynamic disorder in a magnetic material using SEDM.

The SEDM apparatus, shown in Fig. 3, requires two Doppler modulators. One is used to drive the single line Mössbauer source at a constant velocity (CVD), populating the desired nuclear sublevel in the sample. The other velocity transducer is used to record the scattered radiation from the sample by moving a single-line analyzer with a constant acceleration (CAD).

Two things are crucial for a successful SEDM experiment. One is perfect synchronization of the CVD and CAD for the duration of the experiment. This is to ensure that data collection occurs only when the selected transition is being excited and that exactly the same energy for each velocity

[a]Current address: Materials and Chemical Sciences Division, Energy Sciences and Technology Department, Brookhaven National Laboratory, Upton, NY 11973-5000; electronic mail: johan@bnl.gov

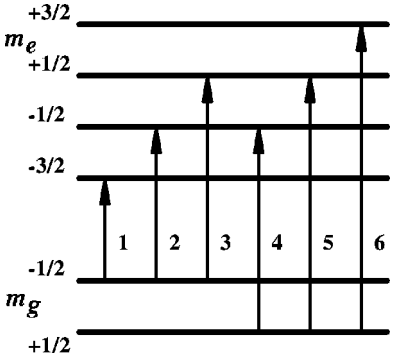

FIG. 1. Energy level diagram of the nuclear energy sublevels for iron.

scan of the CAD is acquired by the multichannel scaler. Early works solved this problem using specially constructed electronics for the transducers and periodic energy calibration.[3–6] Others have used expensive CAMAC technology to solve the transducer synchronization problem.[7] The second requirement is efficient detection of the scattered radiation from the sample. An early SEDM equipment used a single-line $Na_4Fe(CN)_6 \cdot 10H_2O$ absorber attached to the CAD with a standard proportional counter behind it.[3,4] At that time, a high efficiency proportional counter was the simplest method of measuring a signal from the sample. Still, a 2–4 GBq (50–100 mCi) source was necessary for acceptable collection times.

Conversion electron detectors, in principle at least, are sensitive to only resonant photons. Microfoil conversion electron (MICE) detectors are the most sensitive design of conversion electron detector. With multiple, ultrathin ^{57}Fe enriched stainless-steel foils, these detectors offer excellent counting efficiency. A MICE detector designed to be Mössbauer transducer mounted[8] has been built, however, the extreme fragility of foils was not well suited to the constant vibration. Since the bulk of the signal comes from the first foil[9] and increasing the number of foils improves the count rate at the expense of the signal-to-noise ratio, we have built a simple, single foil, drive mounted conversion electron detector (CED). The foil is firmly mounted onto the detector body so that it cannot vibrate. Our CED is both robust, and light enough, to be transducer mounted. With a lower counting efficiency than a MICE detector, this design of a CED still outperforms the counting efficiency of proportional counters by several orders of magnitude.[10]

Wissel[11] Mössbauer transducers use digital-to-analog circuitry, like most modern transducers, and provide outputs which flag various conditions of the constant velocity and constant acceleration wave forms. With this information from the transducers, it was a simple task to design some digital electronic circuits which synchronize the CVD and CAD.

With these ingredients, our SEDM apparatus has provided the necessary upgrade in counting efficiency, with a 1000-[3] to 5000-fold[4] improvement in effective counting time when compared with previous experimental configurations, and the ability to stay synchronized for an indefinite period of time.

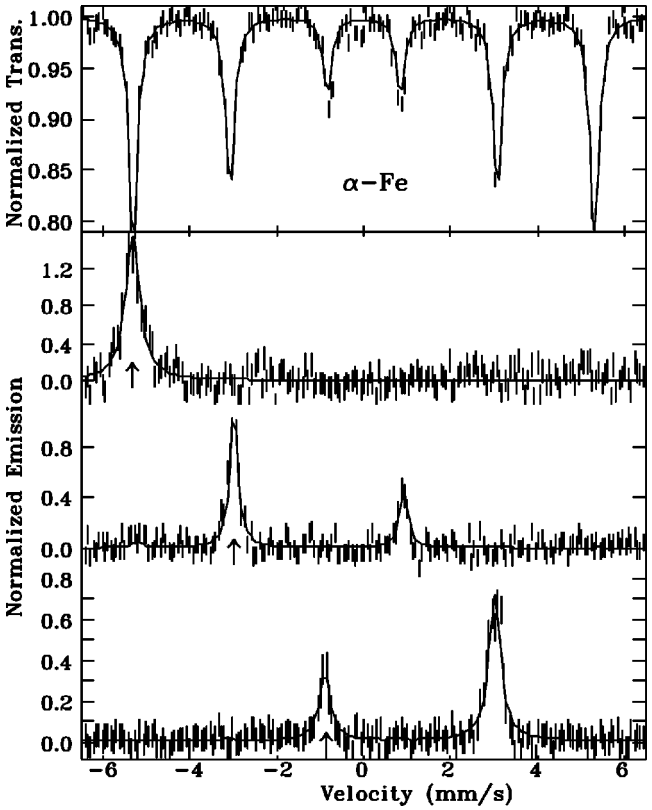

FIG. 2. Transmission Mössbauer spectrum of α-Fe and the SEDM spectra obtained when lines Nos. 1, 2, and 3 are driven (pump energies indicated by the ↑).

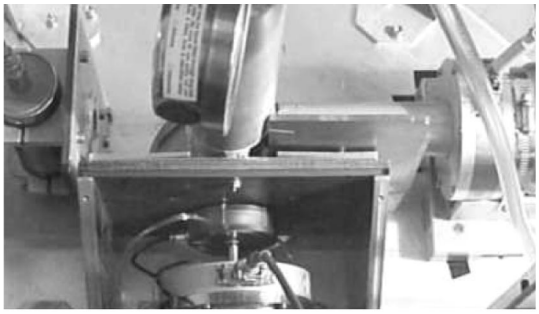

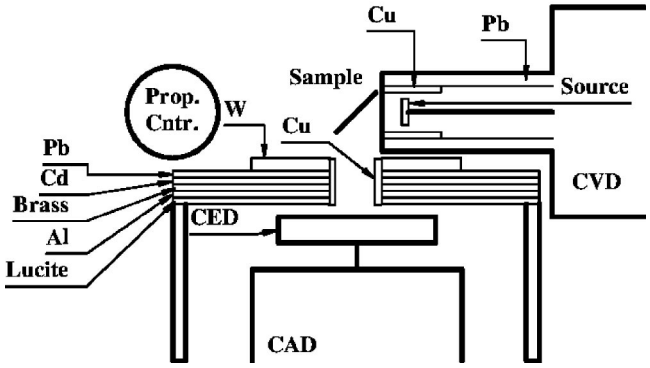

FIG. 3. (Top) Photograph of the SEDM apparatus with the closed cycle refrigeration system. From left to right: Prop. counter, sample in scattering enclosure for the closed cycle refrigerator, CAD with CED behind shielding (bottom center), CVD with source. (Bottom) Schematic block diagram of the SEDM apparatus.

The SEDM equipment was tested on a 25 μm thick α-Fe foil. We have examined the effects of static disorder by examining an amorphous $Fe_{80}B_{20}$ sample.[1] Superparamagnetic relaxation in a Fe_3O_4 ferrofluid[12] has been studied as well, and we are currently investigating spin dynamics in amorphous Fe–Zr and Fe–Sc spin glasses.

II. SPECTROMETER DESIGN AND OPERATION

A photograph and schematic diagram of our SEDM apparatus is shown in Fig. 3. We will discuss the construction and optimization of the CED, synchronization and data collection with the two drives, as well as shielding, in the following subsections. This is followed by a description of the calibration and operation of the SEDM spectrometer.

A. CED

The heart of our improvements to the SEDM technique is the use of a drive mounted CED as our energy analyzer. This offers a tremendous enhancement in counting efficiency.

An orientation of 90° for the energy analyzer with respect to the source is the simplest, and fortunately, most beneficial, geometry to use in a scattering experiment. For a SEDM experiment, this setup solves two problems. One is that it reduces possible coherent Rayleigh scattering to a minimum as these scattering events have a $\cos^2(\theta)$ angular dependence. Another is that the 90° position offers the greatest distance between CVD and CAD, allowing the maximum amount of radiation shielding between source, sample and detector. This is a necessity which we will explain later in Sec. II C.

A detector with too large a collection area will lead to cosine broadening of the spectral lines, so it is necessary to keep the angular acceptance limits of the collected photons to a reasonable minimum. This restricts the photons that we can collect from the sample (which are radiating off the sample in all directions) to a small solid angle. An efficient detector of scattered γ photons from the sample is clearly needed. A CED provides the most efficient means of collecting resonant events from a sample. In general, the relative advantages of a conversion electron detector go up as the magnitude of the absorption from a sample decreases.[9] An emission signal residing over low count background is a more effective detection technique for SEDM then a proportional counter which cannot offer a greater than 10% absorption signal from re-emitted γ photons in a high count background.

A CED is basically a proportional counter with a resonant foil which acts as a cathode and a fine wire biased to a high voltage for an anode. A 14.4 keV γ photon from a SEDM sample will resonantly scatter inside the cathode foil and excite a ^{57}Fe nucleus. Only about 10% of the nuclei will return to their ground states via a re-emitted photon. The other 90% emit a conversion electron followed by an x-ray or Auger electron. On average, two conversion electrons are emitted for each resonant event,[13] so this process offers the greatest possible signal. To reduce the sensitivity of the CED to photons, a fill gas of helium is used. A few percent of a quench gas (in our case methane) is added to the helium, to keep the detector from avalanching from photons scattering off the helium. To reduce the response of a CED to lower energy photons (such as the 6 keV x ray from the decay of a Mössbauer nucleus), a filter material is placed in front of the cathode.

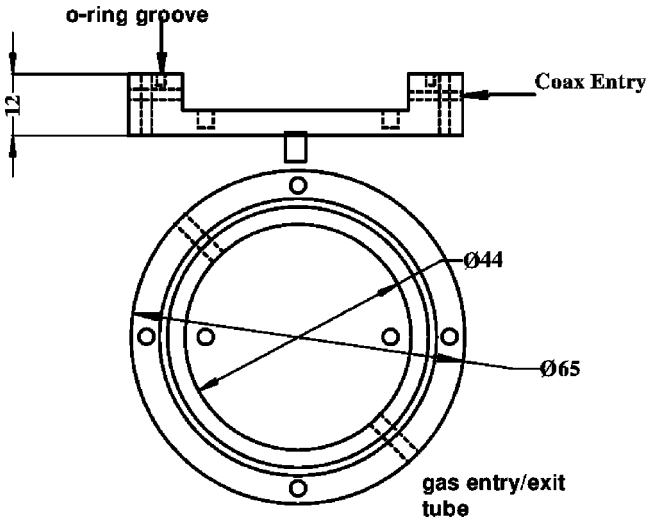

FIG. 4. Sectional views of the detector body. All dimensions in mm.

This CED is based upon a previous design used for Mössbauer source experiments with extremely low doping levels of ^{57}Co.[10] The SEDM CED is more modular, allowing for easy removal of the CED cathode sample, and attention towards sealing the detector has resulted in low He/CH_4 gas flow rates, ensuring consistent and reproducible performance. Low density materials were used throughout the construction which served a twofold purpose. Keeping the mass of the CED to a minimum ($\simeq$40 g for this CED) limited the possibility of adversely affecting the linear acceleration of the CAD. Lower Z materials also reduce the number of nonresonant scattering events that might take place anywhere in the CED during a measurement, diminishing background counts.

Sectional views of the Plexiglas detector body are in Fig. 4. The cover (not shown) is a 65 mm diam, 2 mm thick Plexiglas disk. Plexiglas is light, easy to machine, and is an excellent filter of the unwanted fluorescence from the sample. A 100 mm^2, 90% ^{57}Fe enriched 1.3 μm thick 310 stainless-steel foil[14] is the CED cathode. An enriched foil is used to maximize the possible resonance events from γ photons off the SEDM sample. The foil is clamped firmly in place with a 40 mm diam, $\sim$0.1 mm thick Plexiglas ring with a 9.8 mm diam center hole to expose the cathode to the γ photons from the sample. The anode wire is 25 μm gold-coated tungsten and soldered across the 4 mm sections of the disk shown in Fig. 5. This anode holder is made of 2 mm thick copper-clad circuit board. Facing surfaces of the detector body and cover were polished and an o-ring is used to ensure a seal between detector body and cover. All inner surfaces were fully aluminized and connected to ground. Four nylon screws are used to fasten the cover to the body. A 250 mm long lightweight coaxial cable (RG-174/u) with a gold mini-SMC high voltage connector carries the bias volt-

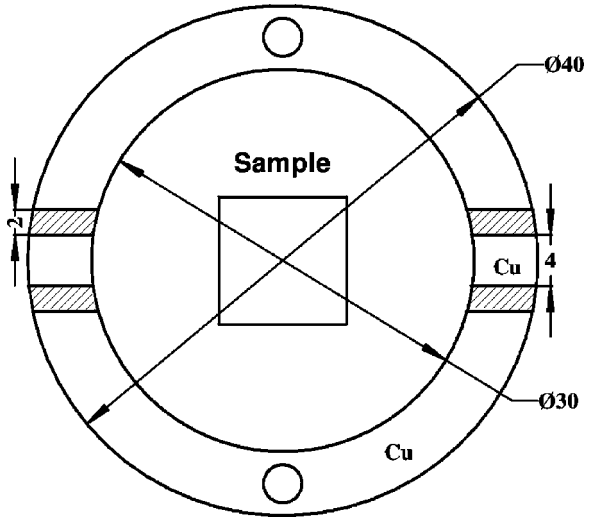

FIG. 5. Sectional view of the anode wire mount made of 2 mm thick copper clad circuit board. All dimensions in mm.

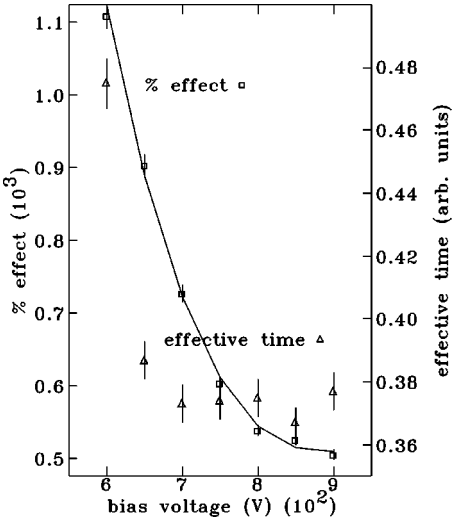

FIG. 7. Effect (ε) and effective counting time t_{eff} as functions of CED bias voltage as described in the text. The solid line is a guide to the eye.

age from the preamp to the anode wire. One end of the SMC connector was threaded into the detector body and the anode wire was soldered onto the center pin of the connector. Thin coax is used to reduce mechanical stiffness which would interfere with oscillating the detector. The He with 4% CH_4 gas mix enters and exits though two 2 mm diam plastic tubes. The premixed gas flows through the detector at a rate of ~ 0.1 cm^3/min. A photograph of the CED mounted onto the CAD during a SEDM experiment is shown in Fig. 3.

The CED was optimized for counting efficiency in the following way. Initially, with the minimum possible lower level discriminator setting, pulse height spectra of the CED on and off resonance were collected at various bias voltages. The pulse height spectra, with the off resonance contribution subtracted, indicated when the conversion electron signal was maximized. Figure 6 shows this trend for several bias voltages, with the 800 V bias showing a clear maximum for the conversion electron signal around channel 100. To confirm this setting, conversion electron Mössbauer spectra of the single line stainless-steel cathode of the CED were collected at different bias voltages. The effect $\varepsilon = I/I_\infty$, where I is the peak intensity and I_∞ is the baseline of the spectrum, was calculated for each spectrum, as well as the following measure of the effective counting time, $t_{\text{eff}} = 2(\varepsilon + 2)/(\varepsilon^2 I_\infty)$.[15] The operating bias voltage for the CED of 700 V exhibited the minimum effective counting time and maximum signal effect, shown in Fig. 7. A spectrum of the enriched stainless-steel cathode is shown in Fig. 8. The CED has an operational linewidth of 0.153 ± 0.002 mm/s, compared to 0.191 ± 0.001 mm/s for a transmission spectrum of a 10 μm thick 310 stainless steel.

Background contributions in the form of detector noise and low-energy photoelectrons were reduced with the proper selection of the lower level discriminator setting for the detector electronics. Using the same method to find the optimal bias voltage, a lower level discriminator setting of 10–12 mV was selected (see Fig. 9).

B. Drive synchronization and data collection

A requirement for SEDM spectroscopy is the synchronization of the CVD and CAD. The energy analyzer must sweep across its range of velocities while the transition is being pumped by the constant velocity drive (CVD) trans-

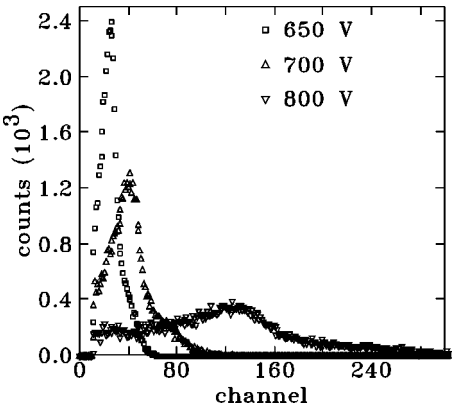

FIG. 6. Pulse height spectra with off resonance background subtracted at various bias voltages for the CED. The conversion electron peak is clearly seen in the 800 V spectrum around channel 100.

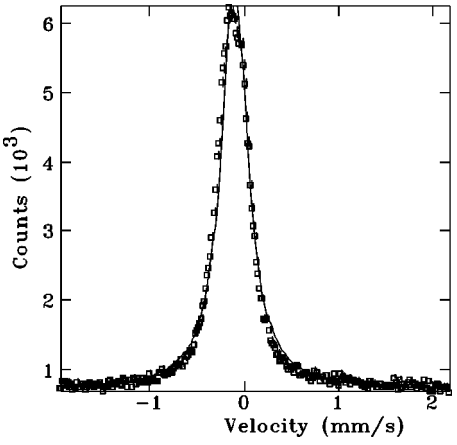

FIG. 8. CED spectrum of the enriched 310 stainless-steel sample. A linewidth of 0.153 ± 0.002 mm/s and an effect of $\approx 800\%$ are substantial improvements over conventional transmission measurements.

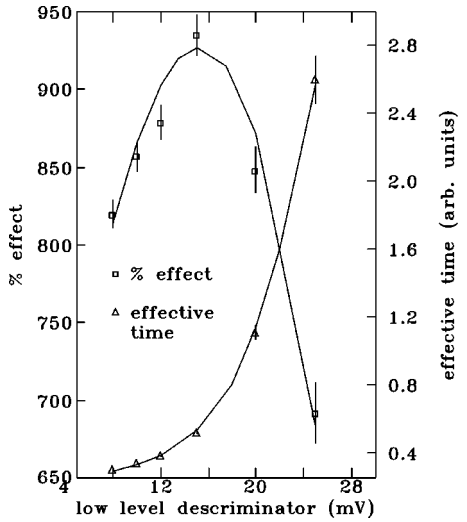

FIG. 9. Effect (ε) and t_{eff} as functions of the lower level discriminator setting for the CED. The solid lines are a guide to the eye.

ducer and exactly the same velocity should be recorded in each channel of the multichannel scaler during a scan. A Wissel[11] velocity transducer MA-260, Mössbauer driving unit MDU-1200 with a digital function generator DFG-1200 was used for the CVD and a Mössbauer velocity transducer MA-260 with a Mössbauer driving unit MR-360 and a digital function generator DFG-1000 was used for the CAD. The drive function generators are essentially digital-to-analog (DA) converters with internal clocks which supply the driving unit with a wave form and provide logic pulses during different parts of the wave form for data collection (e.g., TTL pulses for the channel advance, a start signal denoting the beginning of the wave form and a sign signal for the positive and negative velocities of the drive wave form). The internal clocks of the drive function generators can be disabled and an external TTL stepping pulse can be used to provide the channel advance for DA conversion to the driving unit. This feature allows the two drive systems to be used in a master/slave configuration. With an external channel advance frequency of $\approx$100 kHz (4096 channels$\times$25 Hz drive resonant frequency) the CAD is slaved to the CVD using the circuit shown in Fig. 10. The start signal from the CVD and the sign signal from the CAD ensure that both wave forms begin at their maximum velocities at the same time. To establish synchronization after a drive has been turned off, a reset trigger is provided. The drive function generators are operated in a standard 512 channel/cycle configuration. The CAD uses a triangular, constant acceleration, wave form. To minimize the velocity error of the CVD proportional-integral feedback loop, a square wave form with a 20% sine wave component at the discontinuities (see Fig. 11) is used. Examining the diagram of the CAD and CVD wave forms in Fig. 11, it seems reasonable to have the CAD double its oscillation period so data can be collected during the positive and negative accelerations of the CAD and standard folding of a spectrum can occur to alleviate possible background problems. This was not possible with our Wissel drive units. The servo loop was unable to cope when operating at twice the 25 Hz mechanical resonant frequency.

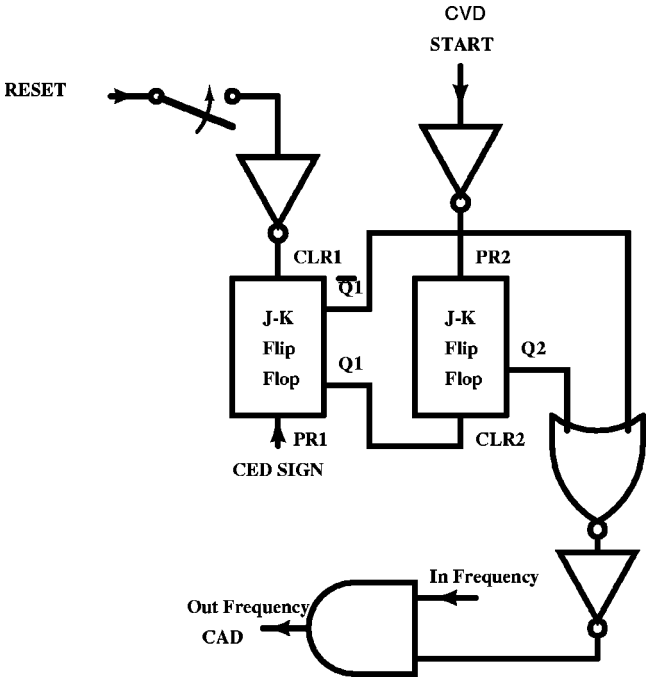

FIG. 10. Schematic of the CVD and CAD synchronization circuit.

The function generators provide a sign signal which indicates when the wave form generates a positive or negative velocity and a count enable signal which establishes when a constant velocity section of the wave form has been reached. With the circuit in Fig. 12, counts from the detector are gated with the CVD sign and count enable signals. This way, signal is collected by the multichannel scaler data acquisition system only when the transition is being pumped by the CVD.

C. Shielding

It is very important when performing SEDM experiments to provide proper shielding of the detector from un-

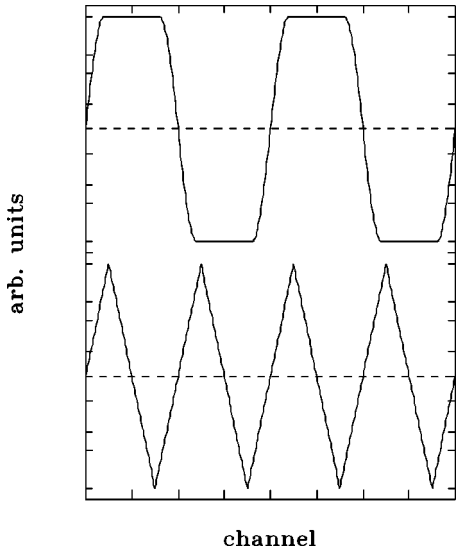

FIG. 11. Diagram of the CVD (top) and CAD (bottom) wave forms used during a SEDM experiment.

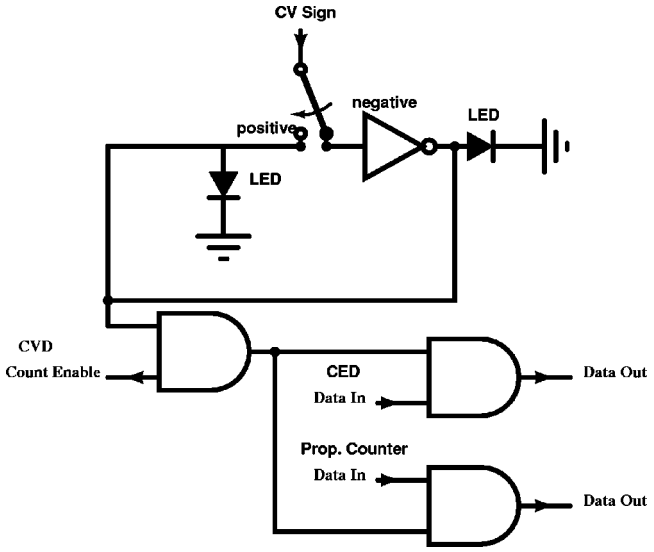

FIG. 12. Schematic of the velocity gating circuit.

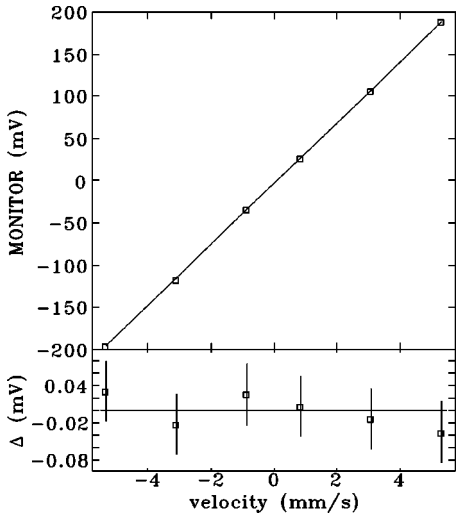

FIG. 13. Velocity calibration of CAD with respect to the six lines of α-Fe. Residuals of the fit (Δ) are shown in the bottom part of the graph.

wanted radiation. Optimum CED performance is achieved with a low background,[9] so keeping nonresonant counts to a bare minimum is crucial.

The biggest source of background counts is line-of-sight photons from the source. The 122 keV γ rays from the nuclear decay of ^{57}Co can penetrate any shielding materials between source and detector. To improve the shielding for the detector, it is better to use many materials with complementary γ-ray absorption coefficients. With this in mind, each metal used for the CED shielding has an absorption coefficient which is optimum for a range of γ-ray energies. The metals are placed in a sequence so photons of lower energies will be absorbed as they scatter on toward the CED. By the time photons have penetrated all the shielding materials, their energies are too low to create photoelectrons in the CED. An example of our shielding is schematically displayed in Fig. 3. 10 mm of tungsten is followed by 10 mm of lead, and then 3 mm of cadmium, 2 mm of brass, 2 mm of aluminum and 3 mm of Plexiglas. Although tungsten has a lower Z then lead, its higher density makes it a better absorber. Collimation of the scattered radiation from the sample is provided by an 11 mm inner diameter copper shell which passes through the shielding and is level with the 10×10 mm cathode. A 2 mm think copper shell sitting inside a 7 mm lead shell shields the source.

D. Operation

Our SEDM apparatus uses standard detector electronics, i.e., detector preamps, high voltage power supplies, multichannel analyzers and rate meters, from ORTEC[16] and Canberra.[17] An Intel-based PC having two ORTEC multichannel scaler (MCS) data acquisition cards collects the spectrum. One MCS card is used to collect counts coming from the CED (the SEDM experiment) and the other MCS card is used for collecting counts from the proportional counter when checking the CVD energy or recording the long term CED stability. The back of the CAD transducer has a source holder. A source is attached here when it is necessary to calibrate the CAD velocities. With a conventional transmission Mössbauer spectrum of the sample in hand, it is a simple task to determine the line energies for a CVD velocity. The experimental procedure for conducting an SEDM experiment is:

(i) Conventional transmission Mössbauer spectra are collected. These spectra are used to determine the transducer velocity for pumping a selected transition. Fits to the transmission spectra offer necessary information to fit SEDM spectra, e.g., distribution of hyperfine fields.

(ii) With the drives synchronized for a SEDM experiment, the CVD energy is tuned across a range of energies centered about the calculated drive velocity and the gated counts from the proportional counter behind the sample are recorded in timed bins (e.g., 100 s/channel). The absorption as a function of drive energy will yield a maximum when the peak of the line is encountered. This is an important check of the CVD energy calculated from the transmission spectrum.

(iii) Once the CVD energy is confirmed, the SEDM experiment begins with one MCS collecting the SEDM spectrum and the other MCS recording the CED counts in timed bins as a check of the detector performance (e.g., the number of counts per bin remains constant for the duration of the experiment).

Since the data gating electronics collect during half of the CVD wave form, no background corrections, typically by folding, are possible. However, with our thin samples as well as source–sample and sample–CED distances of 2–5 cm, flat backgrounds were always measured.

III. SPECTROMETER PERFORMANCE

Using a 1 GBq (25 mCi) ^{57}CoRh source, the SEDM setup was tested on α-Fe. At first, with no calibration for the CVD velocity, all six lines of the α-Fe spectra were found by varying the CVD velocity and recording the absorption of γ rays in the sample. A linear relationship between the ac voltage of the monitor output of the CVD and line positions for α-Fe was demonstrated and used as a calibration of the CVD velocity (Fig. 13).

Collecting a SEDM spectrum while driving line No. 1 of α-Fe provided a strong indication that selective population of the $m_e=-3/2$ nuclear sublevel (shown schematically in Fig. 1) was happening. With the largest cross section, driving line No. 1 would produce the strongest signal, and after approximately 1 day of counting, a single-line SEDM spectrum, shown in Fig. 2, was the result. With a line position of -5.31 ± 0.01 mm/s, in agreement with the line No. 1 energy of α-Fe, the appearance of a single line agrees with the selection rules.

SEDM spectra when the excited states of lines Nos. 2 and 3 in α-Fe were populated established that selective population of a nuclear sublevel was indeed occurring. The population of the $m_e=-1/2$ state results in de-excitations to the $m_g=-1/2$ and $m_g=1/2$ states (see Fig. 1), i.e., pumping line No. 2 yields a spectrum with lines Nos. 2 and 4. When line No. 3 is driven, populating the $m_e=1/2$ state has de-excitations occurring to the $m_g=-1/2$ and $m_g=1/2$ states, resulting in both lines Nos. 3 and 5 in a SEDM spectrum (Fig. 2). This last SEDM spectrum is the most convincing evidence that selective population of the nuclear sublevels is happening, as the de-excitations via the $m_e=1/2\rightarrow m_g=-1/2$ transition has a larger nuclear cross section than the pumped $m_e=1/2$ state, resulting in the return line No. 5 which was *not* pumped having a much greater intensity in the SEDM spectrum than the pumped line No. 3.

To evaluate the SEDM line shape the energy distributions of the source radiation and scattered radiation from the sample as well as the detector energy resolution are required. These items are characterized by their linewidths. Including the energy distribution of the source $\Gamma_{\mathrm{CED}}=0.153\pm0.002$ mm/s, collected in a transmission geometry, describes the energy resolution of the CED. A measure of the source energy distribution is given by the inner lines (Nos. 3 and 4) of a α-Fe transmission spectrum, $\Gamma_s=0.120\pm0.001$ mm/s, which defines the excitation process of a Mössbauer nucleus in the source and the subsequent de-excitation. With this information, a SEDM model assuming Lorentzian line shapes and a single hyperfine field, corrected for the CED isomer shift, was used to fit the α-Fe SEDM spectra. These spectra required approximately 1 day counting times, and exhibit a 3 order of magnitude improvement in counting efficiency over previous experiments.[3,4]

IV. EXAMPLES OF APPLICATION

We are currently using SEDM to separate static and dynamic magnetic disorder in paramagnetic and superparamagnetic systems. To demonstrate the effects of static disorder, SEDM spectra of the metallic glass $Fe_{80}B_{20}$ when driving lines Nos. 1 and 2, were collected. Figure 14 presents the transmission Mössbauer and SEDM spectra of $Fe_{80}B_{20}$ at room temperature (0.45 T_c). The transmission spectrum exhibits the usual broadened six-line pattern of a metallic glass with a broad hyperfine field distribution $P(B_{\mathrm{hf}})$. SEDM data obtained driving lines Nos. 1 and 2 show a single broad line which may be fitted assuming the same $P(B_{\mathrm{hf}})$ determined from the transmission spectrum. From the distribution of hyperfine fields, a range of transitions can now be pumped by the source during the SEDM experiment. Γ_s and $P(B_{\mathrm{hf}})$ correctly predict the SEDM line shapes with fitted linewidths of 0.165 ± 0.002 mm/s, which includes the CED energy resolution, describing the energy distribution of scattered radiation from the sample. These SEDM fits indicate that only part of the hyperfine field distribution is being probed by the SEDM experiment. Compare the narrower SEDM linewidths to

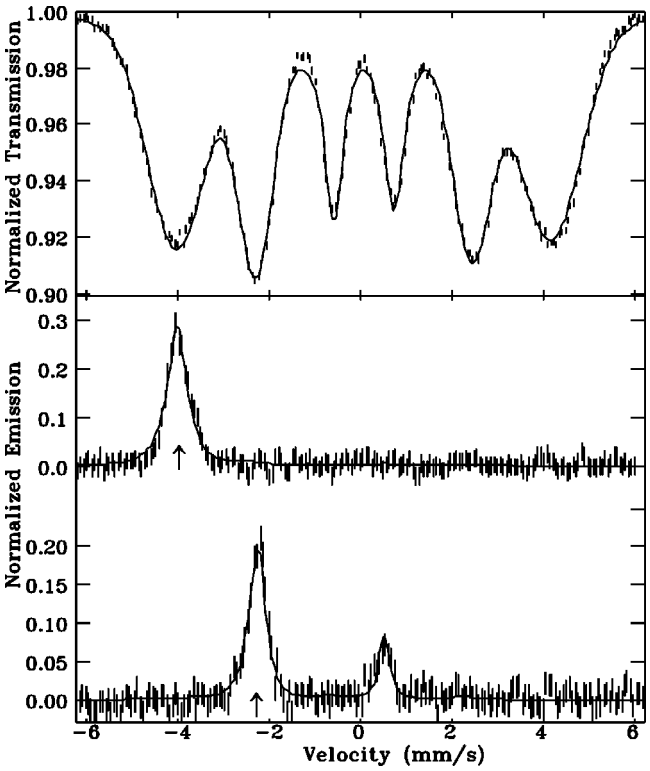

FIG. 14. Transmission Mössbauer spectrum of $Fe_{80}B_{20}$ and SEDM spectra when lines Nos. 1 and 2 are driven (pump energies indicated by the ↑).

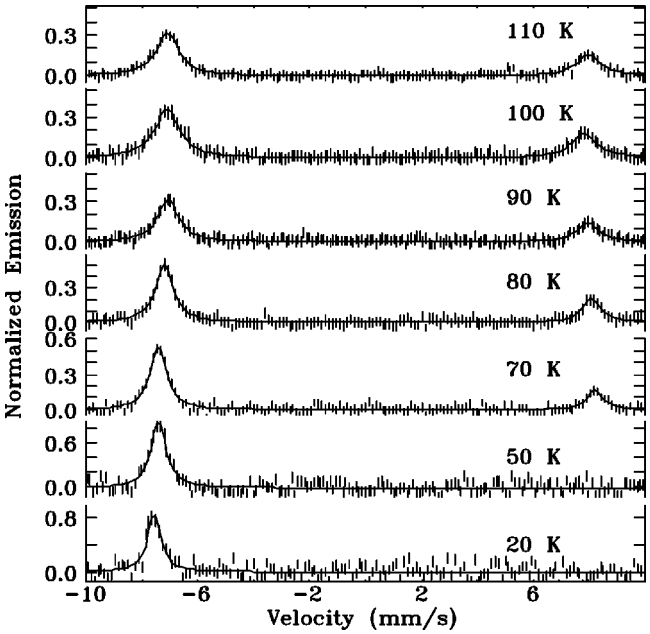

FIG. 15. SEDM spectra of a Fe_3O_4 ferrofluid when line No. 1 is driven at different temperatures. Notice the appearance of line No. 6 above 50 K when superparamagnetic spin flips start happening.

those from the individually fitted lines of the transmission spectrum of $Fe_{80}B_{20}$; line No. 1 gives 0.71 ± 0.02 mm/s and line No. 2 0.39 ± 0.01 mm/s. This is direct evidence that static disorder can be detected using SEDM spectroscopy. The effects of superparamagnetic spin flips of magnetic moments in a Fe_3O_4 ferrofluid upon SEDM spectra[12] are shown in Fig. 15. These SEDM spectra display a striking new phenomena: a new line, not available via the normal, static selection rules (Fig. 1), appears. This is possible because when a spin flip occurs in a particle where we have pumped a nucleus into the $m_{I_e} = -3/2$ excited state, the field within that particle reverses, the projection of I_e onto that field changes sign and the populated state becomes $m_{I_e} = +3/2$. This state then decays to give the line at $\sim +8$ mm/s. The observation of a *sharp* line at $+8$ mm/s, indicates that the moment reversal is instantaneous on the time scale of the SEDM measurement.

V. DISCUSSION

We have constructed a SEDM system using standard transmission Mössbauer equipment and a vibration-free, drive mounted conversion electron detector. The instrument provides easy tuning to the excitation energy of a nuclear sublevel in a sample for the CVD. Radiation shielding and collimation are of simple construction and have been readily customized for different experimental conditions. The SEDM equipment has performed flawlessly for month-long runs, establishing its long term stability. With this drive mounted CED, SEDM need no longer be a fringe technique, and can be applied to problems of current interest, such as spin dynamics,[12] magnetically disordered systems[1] and spin glasses.

ACKNOWLEDGMENTS

The authors would like to thank Dr. A. Kuprin for helping with CED design and optimization and L. Cheng for sputtering aluminum onto the detector components. This work was supported by grants from the Natural Sciences and Engineering Research Council of Canada and Fonds pour la Formation de Chercheurs et l'Aide à la Recherche, Québec.

[1] J. van Lierop and D. H. Ryan, J. Appl. Phys. **85**, 4518 (1999).
[2] D. G. Rancourt, H. H. A. Smit, and R. C. Thiel, J. Magn. Magn. Mater. **66**, 121 (1987).
[3] N. D. Heiman and J. C. Walker, Phys. Rev. **184**, 281 (1969).
[4] B. Balko and G. R. Hoy, Phys. Rev. B **10**, 36 (1974).
[5] J. J. Bara, Phys. Status Solidi A **63**, 119 (1981).
[6] D. C. Price and A. M. Stewart, Hyperfine Interact. **42**, 1157 (1988).
[7] V. G. Semenov, S. M. Irkaev, and Y. N. Maltsev, Nucl. Instrum. Methods Phys. Res. B **95**, 253 (1995).
[8] S. Bocquet, R. J. Pollard, and J. D. Cashion, Hyperfine Interact. **58**, 2503 (1990).
[9] J. G. Mullen and J. Stevenson, Nucl. Instrum. Methods **153**, 77 (1978).
[10] L. X. Liao, D. H. Ryan, and Z. Altounian, Rev. Sci. Instrum. **64**, 679 (1993).
[11] Wissenschaftliche Elektronic GMBH, Piloty Str 3 D-8130 Starnberg, West Germany.
[12] J. van Lierop and D. H. Ryan, Phys. Rev. Lett. **85**, 3021 (2000).
[13] J. J. Spijkerman, Mössbauer Effect Methodology **7**, 85 (1971).
[14] Catalog No. NER-512, Supplied by NEN/DuPont, North Billerica, MA.
[15] A. P. Kuprin and A. A. Novakova, Nucl. Instrum. Methods Phys. Res. B **62**, 493 (1992).
[16] EG&G ORTEC, 100 Midland Road, Oak Ridge, TN 37830.
[17] Canberra Industries, Inc., One State Street, Meriden, CT 06450.